MnO_2 Nanorod Supported Gold Nanoparticles with Enhanced Activity for Solvent-free Aerobic Alcohol Oxidation

Lu-Cun Wang, Yong-Mei Liu, Miao Chen, Yong Cao,* He-Yong He, and Kang-Nian Fan

Department of Chemistry and Shanghai Key Laboratory of Molecular Catalysis and Innovative Materials, Fudan University, Shanghai 200433, People's Republic of China

Received: November 30, 2007; In Final Form: February 20, 2008

Gold nanoparticles supported on β-MnO_2 with different morphologies, i.e., nanorods and conventional particulates, were prepared by homogeneous deposition−precipitation using urea as the precipitation agent. The catalysts were extensively characterized by a combination of different techniques (N_2 adsorption, X-ray diffraction (XRD), transmission electron microscopy (TEM), hydrogen temperature-programmed reduction (H_2-TPR), and X-ray photoelectron spectroscopy (XPS)) in relation to their performance for liquid-phase aerobic oxidation of benzyl alcohol under solvent-free conditions. TEM analysis showed that the two types of gold catalysts have similar gold particle size distributions. TPR results indicated that the presence of Au strongly promotes MnO_2 reduction in the Au/MnO_2-R system. XPS revealed both reduced and oxidized Au species on the MnO_2 nanorods support before and after the reaction. Significantly enhanced catalytic activity was observed for gold catalyst supported on MnO_2 nanorods, as compared with that on commercial MnO_2 powders. The enhanced catalytic activity of the Au/MnO_2-R catalyst was attributed to the beneficial presence of higher amount of oxidized gold species and surface oxygen vacancies resulting from the strong interaction between Au and the well-defined reactive surface of MnO_2 nanorods.

1. Introduction

Supported gold catalysts have attracted significant attention in the last 2 decades owing to their unique catalytic properties under mild conditions.[1−4] Studies on Au catalysts have been mainly focused on gas-phase oxidation, such as CO oxidation, hydrocarbon combustion, selective oxidation, and water gas shift (WGS) reaction.[1−4] It is generally agreed that the catalytic activity of gold catalysts depends on the size of the gold particles, but the nature of the support material, the preparation method, and the activation procedure have also been suggested to play a key role.[1−8] Exceptionally high activities for oxidation of CO have been reported for highly dispersed Au on reducible oxides, such as TiO_2, Fe_2O_3, and CeO_2, etc. It has been proposed that the reducible metal oxide support supplies oxygen to form active oxidic gold sites.[8] Sites at the gold−support interface have also been claimed to be responsible for the activity in CO oxidation.[9−11] Other explanations focus on the charge transfer between the support, particularly negatively charged defects (F centers), and the Au particles.[12] In addition, the effects of low-coordinated sites and surface roughness have also been suggested.[11,13−15]

Over the past decade, much attention has also been paid to the application of gold catalysts in the liquid phase, in particular for the selective oxidation of alcohols, due to its importance in both fine chemicals industry and academia.[3] The substrates investigated to date include aromatic, aliphatic, and allylic alcohols, both primary and secondary alcohols, and some polyols.[16−21] In most cases, supported gold catalysts show high catalytic activity with much higher selectivity at low temperature and better stability than Pd or Pt catalysts.[16] Moreover, it has been shown that choice of suitable metal oxide as support plays an important role in determining the catalytic activity and selectivity of gold catalyst.[17,18,20] For example, it was found that compared with activated carbon or graphite, metal oxides such as CeO_2 or TiO_2 supported gold catalysts are more active and selective toward the solvent-free oxidation of alcohols to their corresponding aldehydes or ketones.[17,18] Notably, Abad et al. have recently reported that Au nanoparticles supported on nanocrystalline CeO_2 were extraordinarily active and selective for the solvent-free oxidation of various alcohols to ketones, as compared with the conventional CeO_2.[17]

Featured with superior ability to activate and supply oxygen, manganese oxide is well-known as a stoichiometric oxidant for oxidation of hydrocarbons in organic synthesis and has also been extensively investigated as an excellent support or promoter for various metal or metal oxide catalysts.[22−27] When combined with gold nanoparticles, significantly enhanced activity has been achieved over the Au/MnO_x system for low-temperature CO oxidation in the absence or presence of H_2 for fuel cell applications. However, to the best of our knowledge, manganese oxide has rarely been addressed as support of gold nanoparticles in the liquid-phase catalytic oxidation reactions.[20,27] The present work focuses on the exploring of the potential of MnO_2 material in the gold-catalyzed oxidation of various structurally different alcohols by molecular oxygen. Special attention is paid to the effects of support morphology on their structural properties and catalytic behavior in the process of aerobic alcohol oxidation. The structure−activity relationships of the Au/MnO_2 materials are discussed in light of a detailed characterization of the physicochemical and surface properties of the catalysts.

2. Experimental Section

2.1. Preparation of Supports and Catalysts. The β-MnO_2 nanorods were prepared by hydrothermal method according to

* Corresponding author. Phone: +86-21-55665287. Fax: +86-21-65642978. E-mail: yongcao@fudan.edu.cn.

10.1021/jp711333t CCC: $40.75
Published on Web 04/09/2008

the reported procedure.[28] Briefly, $MnSO_4 \cdot H_2O$ (0.008 mol) and an equal amount of ammonium persulfate ($(NH_4)_2S_2O_8$) were put into distilled water at room temperature to form a homogeneous solution, which was then transferred into a 40 mL Teflon-lined stainless steel autoclave, sealed and maintained at 140 °C for 24 h. After the reaction was completed, the resulting solid product was recovered by filtration and washing four times with distilled water. Gold (5.0 wt %) was deposited on as-synthesized β-MnO_2 nanorods (denoted as Au/MnO_2-R) by homogeneous deposition−precipitation (HDP) using urea as the precipitating agent.[29] In a typical procedure, 3.6 g urea was dissolved in 200 mL of 1.46 mmol/L $HAuCl_4$ solution (urea/Au = 100, molar ratio) at room temperature. An amount of 0.55 g of MnO_2 support was then added to this clear solution, and the temperature of the resulting slurry was increased gradually to 90 °C. The temperature was maintained for 4 h, followed by filtering and washing several times with distilled water. The solid product was dried overnight before calcination at 300 °C for 4 h in static air. For comparison, a gold catalyst supported on commercial MnO_2 (Sinopharm Chem. Reagent., 99.9%) (denoted as Au/MnO_2-C) was also prepared following the same procedure. Elemental analysis results showed that the gold loadings were 5.0 wt % for both catalysts.

Reference gold catalysts including 1.5 wt % Au/TiO_2 (type A, lot no. Au/TiO_2 no. 02-1), 4.5 wt % Au/Fe_2O_3 (type C, lot no. Au/Fe_2O_3 no. 02-5), and 0.8 wt % Au/C (type D, lot no. Au/C no. 38D) were supplied by the World Gold Council (WGC).[30]

2.2. Catalyst Characterization. The BET specific surface areas of the calcined catalysts were determined by adsorption−desorption of nitrogen at liquid nitrogen temperature, using a Micromeritics TriStar 3000 equipment. Sample degassing was carried out at 300 °C prior to acquiring the adsorption isotherm.

Elemental analysis with respect to Au loading was performed using inductively coupled plasma atomic emission spectroscopy (ICP-AES) on a Thermo Electron IRIS Intrepid II XSP spectrometer. The samples were dissolved in a mixture of concentrated HCl and HNO_3 with volumetric ratio of 3:1 prior to the analysis.

The X-ray powder diffraction (XRD) of the samples was carried out on a Bruker D8 Advance X-ray diffractometer using nickel-filtered Cu Kα radiation with a voltage and current of 40 kV and 20 mA, respectively.

Transmission electron microscopy (TEM) images were recorded on a JEOL 2011 electron microscope operating at 200 kV. Before being transferred into the TEM chamber, the samples dispersed with ethanol were deposited onto a carbon-coated copper grid and then quickly moved into the vacuum evaporator.

Temperature-programmed reduction (TPR) profiles were obtained on a homemade apparatus loaded with 20 mg of catalyst. TPR experiments were carried out in 5% H_2/Ar flowing at 40 mL·min^{-1}, with a ramping rate of 10 °C·min^{-1} to a final temperature of 650 °C. The H_2 consumption was monitored using a TCD detector.

X-ray photoelectron spectroscopy (XPS) spectra were recorded with a Perkin-Elmer PHI 5000C system equipped with a hemispherical electron energy analyzer. The Mg Kα source ($h\nu$ = 1253.6 eV) was operated at 15 kV and 20 mA. The binding energy (BE) scale was referenced to the C 1s peak (284.6 eV) arising from adventitious carbon in the sample.

2.3. Catalytic Activity Tests. The liquid-phase aerobic oxidation of alcohols was carried out in a high-pressure, Teflon-lined, stainless steel autoclave reactor (Dalian Tongchan Co. Ltd, China; 200 mL). Typically, 0.2 g of the catalyst was added to the catalytic reactor charged with 200 mmol of alcohols. The reactor was sealed and purged five times with oxygen before reaction. The consumed O_2 was replenished by maintaining the oxygen pressure constant throughout the experiment. The magnetic stirring speed was set at 1200 rpm, and the reaction mixture was raised to the required temperature. Samples were taken periodically during the reaction. The products were separated by centrifuging and analyzed by a gas chromatograph (Trace GC Ultra) fitted with an HP-5 capillary column (25 m × 0.32 mm) and flame ionization detector (FID). The conversions and selectivities were determined using undecane as an internal standard in all reactions.

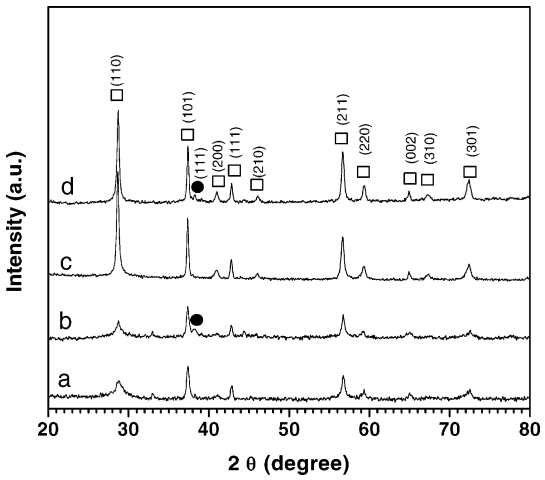

Figure 1. XRD patterns of (a) MnO_2-C, (b) Au/MnO_2-C, (c) MnO_2-R, and (d) Au/MnO_2-R. (□) β-MnO_2, (●) Au^0.

3. Results and Discussion

3.1. Structural and Textural Properties of the Catalysts. The XRD patterns given in Figure 1 show that the two MnO_2 materials have identical diffraction features characteristic of the β-MnO_2 phase (JCPDS 24-0735). However, the relative intensity of the peak corresponding to the (110) plane for MnO_2 nanorods is much higher than that for the commercial MnO_2 particles. According to Xu et al.,[31] the preferential plane exposed by a particle depends substantially on the shape of the particle. Therefore, this observation confirms a disparity in the shape of the MnO_2 supporting materials, pointing to a preferential exposure of the (110) plane in the nanorod samples.[28] After the deposition of gold nanoparticles on the surface of MnO_2 supports, the XRD patterns remain unchanged, although weak metallic gold diffraction lines are evidenced.

TEM images shown in Figure 2A further reveal that the MnO_2 nanorods have well-defined rodlike morphology with diameters of 40−100 nm and lengths ranging between 2.5 and 4.0 μm. The high-resolution TEM (HRTEM) image (Figure 2B) shows that the MnO_2 nanorods are characteristic of single-crystalline nature and possess the (110) planes as the main surfaces. The structure feature of MnO_2 nanorods remained after depositing Au. As shown in Figure 2, parts C and E, Au nanoparticles are highly dispersed on the MnO_2 surface, and the size distribution ranged from 2.0 to 10.0 nm for both catalysts as depicted in Figure 2F. Accordingly, on the basis of 200 particles, the mean gold particle sizes are estimated to be 4.4 and 5.0 nm for Au/MnO_2-R and Au/MnO_2-C, respectively. In addition, the HRTEM image of the Au/MnO_2-R catalyst (Figure 2D) shows that the gold nanoparticles on the surface of MnO_2 nanorods are mainly semispherical in shape.

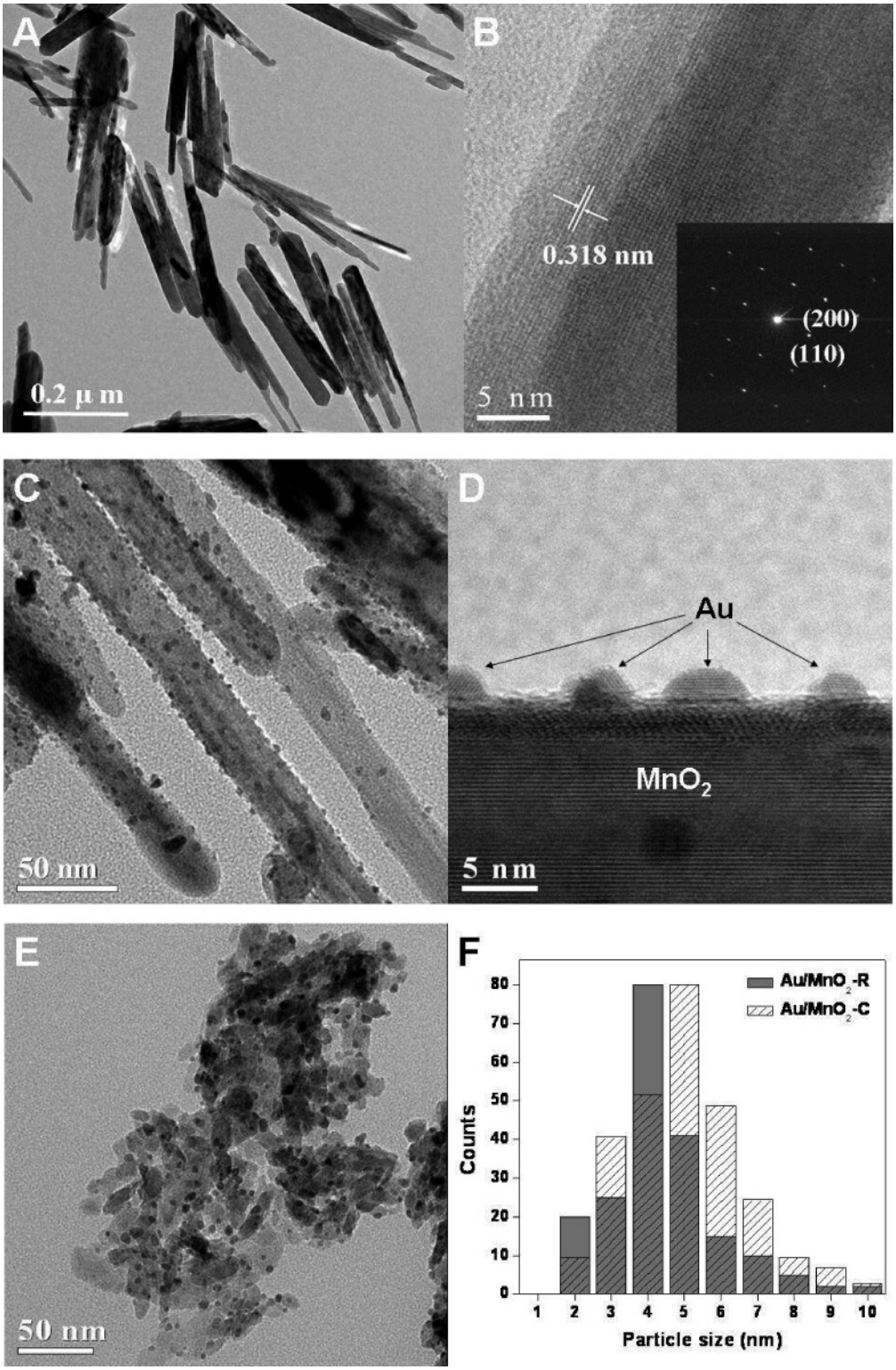

Figure 2. (A) TEM image of pure MnO_2 nanorods; (B) HRTEM image and electron diffraction pattern (inset) of MnO_2 nanorod. In the HRTEM image, the spacing between the lattice fringes is ca. 0.32 nm, which corresponds well with the (110) crystal plane of β-MnO_2 (pyrolusite). (C) TEM image of Au/MnO_2-R catalyst; (D) HRTEM image of Au/MnO_2-R catalyst. (E) TEM image of Au/MnO_2-C; (F) size distributions of Au nanoparticles obtained for Au/MnO_2-R and Au/MnO_2-C.

3.2. Redox Properties and Chemical States. TPR experiments were carried out to investigate the reducibility of the various MnO_2-based materials. Figure 3 presents the reduction profiles of MnO_2 nanorods, commercial MnO_2, and their corresponding supported gold catalysts. Two reduction peaks are observed for all four samples, indicating the stepwise reduction of manganese oxides.[32] The sample MnO_2-R exhibits a significantly narrower peak and lower reduction temperature as compared with MnO_2-C. With Au introduction, the low-temperature (LT) reduction peak of the Au/MnO_2-R catalyst shifted dramatically from 325 to 178 °C, whereas much less variation is achieved for that of Au/MnO_2-C, viz., from 365 to 313 °C. These results clearly demonstrate that the presence of Au nanoparticles strongly promotes MnO_2 reduction, with such promotion effect being more pronounced for the Au/MnO_2-R than Au/MnO_2-C system. The reduction of MnO_2 material was

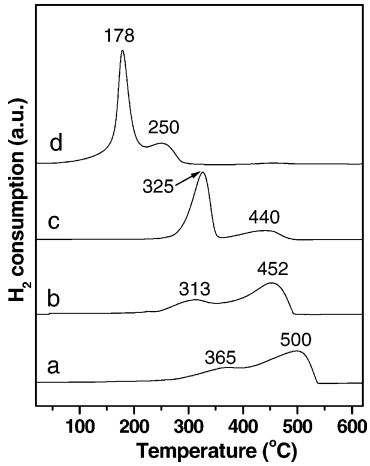

Figure 3. TPR profiles of MnO_2 materials before and after the introduction of gold: (a) MnO_2-C, (b) Au/MnO_2-C, (c) MnO_2-R, and (d) Au/MnO_2-R.

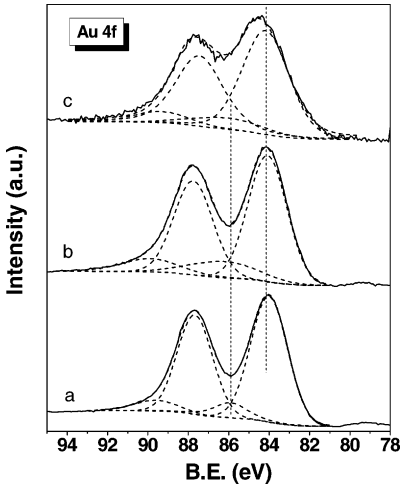

Figure 4. Au 4f XPS spectra of MnO_2 supported gold catalysts: (a) Au/MnO_2-C; (b) Au/MnO_2-R; (c) used Au/MnO_2-R.

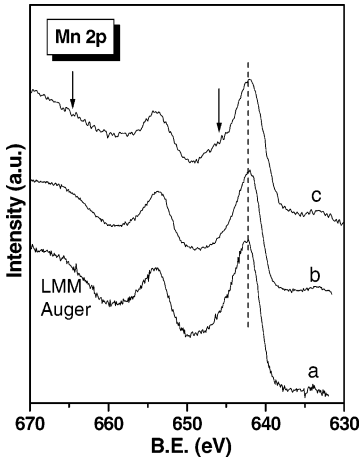

Figure 5. Mn 2p XPS spectra of MnO_2 supported gold catalysts: (a) Au/MnO_2-C; (b) Au/MnO_2-R; (c) used Au/MnO_2-R.

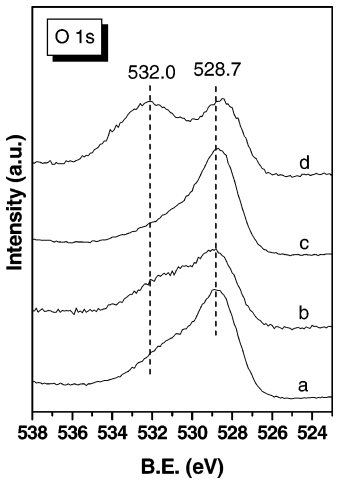

Figure 6. O 1s XPS spectra of (a) MnO_2-C, (b) Au/MnO_2-C, (c) MnO_2-R, and (d) Au/MnO_2-R.

also shown to be strongly facilitated by the presence of Ag[31] and Rh,[33] which has been attributed to the occurrence of spillover phenomena involving either hydrogen activated on the metal phase or lattice MnO_2 oxygen induced by intimate metal−support interactions.

The catalyst surface composition and oxidation state were investigated by XPS. Figures 4 and 5 show the Au 4f and Mn 2p core level XPS spectra of various MnO_2 supported gold catalysts, respectively. To study the surface structural changes that may occur during the oxidation reaction, the Au 4f and Mn 2p XPS spectra of Au/MnO_2-R catalyst after removal from the reactor are also included. The detailed XPS parameters of all samples are summarized in Table 1. Broad peaks of Au $4f_{7/2}$ and Au $4f_{5/2}$ states are observed in all Au/MnO_2 samples, indicating the presence of both metallic and ionic gold species.[34,35] As shown in Figure 4, the variation in the relative intensity at ca. 84 eV indicates the presence of different amounts of Au^0 species in the two Au/MnO_2 catalysts. Deconvolution analysis results show that, in addition to the main peak characteristic of metallic Au^0, the XPS spectra also contain the $4f_{7/2}$ signals from $Au^{\delta+}$ ions.[36−38] As shown in Table 1, the fraction of $Au^{\delta+}$ species, probably at the gold−support interface, in the Au/MnO_2-R catalyst (18.5%) is evidently larger than that of the Au/MnO_2-C catalyst (11.8%). Furthermore, it is worthwhile to note that oxidized gold species (15.6%) were also detected on the surface of Au/MnO_2-R catalyst after reaction for 8 h in the solvent-free oxidation of benzyl alcohol. Notably, this contribution is insignificantly decreased after reaction, suggesting that ionic gold has suffered modest reduction during the reaction. Similar to our findings, the presence of positive gold species along with metallic Au have also been reported in Au/CeO_2 and Au/$Cu_5Mg_1Al_2O_x$ catalysts for selective oxidation of alcohols.[17,21]

The XPS spectra shown in Figure 5 indicate that the Mn $2p_{3/2}$ peaks of both Au/MnO_2-C and Au/MnO_2-R samples have a BE of about 642.1 eV, which is in good agreement with those reported in the literature for MnO_2, i.e., 642 ± 0.2 eV.[39] Moreover, a weak shoulder can be identified at about 646 eV, the intensity of which is slightly stronger for sample Au/MnO_2-C as compared with Au/MnO_2-R, as indicated by the two arrows. The shoulder feature at ca. 646 eV is due to the presence of MnO, whereas the characteristic feature at 663 eV is related to Mn species associated with lower valence states, i.e., Mn_3O_4 or Mn_2O_3.[40] These results point to the presence of a high concentration of oxygen vacancies on the surface of Au/MnO_2 catalysts. After the oxidation reaction, the 646 eV shoulder feature becomes even more distinct along with the disappearance of the satellite feature near 663 eV. This may imply that slight reduction of the MnO_2 support had occurred during reaction.

TABLE 1: XPS Results of Pure MnO_2 and Supported Gold Catalysts

catalyst	BE of Au $4f_{7/2}$ (eV)	fraction of Au species (%)	Au/Mn molar ratio	O_T/Mn molar ratio[a]	O_L/Mn molar ratio[b]
MnO_2-C				2.4	1.8
MnO_2-R				2.3	1.7
Au/MnO_2-C	84.0	88.2	0.24	2.6	1.7
	85.9	11.8			
Au/MnO_2-R	84.1	81.5	0.26	4.2	1.4
	86.2	18.5			
Au/MnO_2-R[c]	83.9	84.4	0.22	7.7	1.1
	86.0	15.6			

[a] O_T, total surface oxygen. [b] O_L, surface lattice oxygen. [c] Used catalyst, after reaction for 8 h in the solvent-free oxidation of benzyl alcohol.

Similar observations have been reported in an XPS investigation of Au/MnO_x catalysts prepared by coprecipitation.[41]

The O 1s XPS spectra obtained from MnO_2 and the supported gold catalysts are depicted in Figure 6. The O 1s main peak at ca. 528.7 eV is attributed to the lattice oxygen bonded to Mn atoms.[41−43] In addition, distinct shoulders are visible on the high BE sides of the main peaks, which were assigned to a mixture of hydroxyl groups and adsorbed water on the surface of catalysts.[40,41,43] As shown in Figure 6, with the introduction of gold, the intensities of the shoulder features at higher binding energies significantly increased, pointing to the enrichment of hydroxyl groups and accumulation of adsorbed water on the surface induced by the gold−support interaction. Moreover, the shoulder peak in the O 1s XPS spectrum of Au/MnO_2-R catalyst is apparently stronger than that of Au/MnO_2-C, indicating higher tendency to form hydroxyl groups or adsorb water molecules on the surface of Au/MnO_2-R catalyst.

The surface compositions in terms of Au/Mn and O/Mn molar ratios are summarized in Table 1. It is clear that the molar ratio of the total amount of surface oxygen (O_T) to Mn is significantly higher than the stoichiometric value in the MnO_2 materials. Moreover, a pronounced increase in the O_T/Mn ratio is identified for the Au-containing samples. All these results further corroborate the presence of a higher concentration of oxygen-containing adsorbates, most likely hydroxyl groups or water, on the surface of Au/MnO_2 catalysts, especially for sample Au/MnO_2-R. The peak deconvolution of the O 1s lines gives more information about the relative amount of different surface oxygen species. As shown in Table 1, the molar ratios of surface lattice oxygen (O_L, 528.7 eV) to Mn for all samples are smaller than the stoichiometric value in MnO_2, inferring the presence of oxygen vacancies on the surface of the catalysts. Notably, the O_L/Mn ratio of MnO_2-R decreases from 1.7 to 1.4 after the introduction of gold. In contrast, little discernible change of the O_L/Mn ratio is observed for Au/MnO_2-C catalyst. In addition, the O_T/Mn ratio of the spent Au/MnO_2-R catalyst is much higher than that of the fresh catalyst. This may result from the adsorption of reactant or other oxygen-containing organic molecules on the surface of the catalyst, while the lower O_L/Mn ratio is consistent with the partial reduction of MnO_2 support as indicated above.

3.3. Solvent-free Aerobic Oxidation of Alcohols. For the MnO_2 supported gold catalysts, our initial studies focused on the oxidation of benzyl alcohol because this reaction is often employed as a model reaction for alcohol oxidation.[18−20] Furthermore, this molecule was chosen because of its relatively high reactivity and because the main product is a nonenoliable aldehyde thus reducing the number of possible side products.[21] In all cases, benzaldehyde was obtained as the major product, and only small amounts of other product, viz., benzyl benzoate, were observed. Abad et al. have shown by H^1 NMR spectroscopy that the ester was directly formed via the hemiacetal intermediate.[17] However, it cannot be excluded that that the instant reaction between benzoic acid (the overoxidized product, which was not detected in our experiments) and the reactant (benzyl alcohol) may also contribute to some extent toward the ester formation, as suggested by Choudhary et al.[44]

TABLE 2: Comparison of the Catalytic Performance of Various Gold Catalysts in the Solvent-free Oxidation of Benzyl Alcohol to Benzaldehyde[a]

catalyst	Au loading (wt %)	substrate/Au ratio	conversion (%)	selectivity (%)	yield (%)
MnO_2-R			1.9	99.2	1.9
MnO_2-C			1.1	99.5	1.1
Au/MnO_2-R	5.0	3940	40.7	98.6	40.1
Au/MnO_2-C	5.0	3940	13.6	97.8	13.3
Au/Fe_2O_3[b]	4.5	3945	9.8	99.3	9.7
Au/TiO_2[c]	1.5	3950	30.5	99.6	30.2
Au/C[d]	0.8	3955	20.6	99.5	20.5

[a] Reaction conditions: 200 mg of catalyst, 200 mmol of benzyl alcohol, 0.3 MPa of O_2, 120 °C, reaction for 5 h. [b] Catalyst amount: 222 mg. [c] Catalyst amount: 665 mg. [d] Catalyst amount: 1245 mg.

The catalytic results obtained in the solvent-free liquid-phase oxidation of benzyl alcohol to benzaldehyde by molecular oxygen at 120 °C over various catalysts are presented in Table 2. Control experiments using the parent MnO_2 supports (substrate to MnO_2 ~100) in the absence of gold demonstrate that only less than 2% of the benzyl alcohol can be oxidized to benzaldehyde within 5 h at 120 °C, confirming the stoichiometric oxidant nature of the MnO_2 materials and the essential role of Au for catalytic alcohol oxidation.[45−47] Apparently, results given in Table 2 show that the surface structural properties of the MnO_2 support have a significant influence on the activity of Au/MnO_2 catalysts. The conversion of benzyl alcohol after reaction for 5 h over Au/MnO_2-R was 40.5%, about 3 times higher than that on Au/MnO_2-C, i.e., 13.6%, whereas the selectivity to benzaldehyde was always higher than 98%. Moreover, as shown in Table 2, the catalytic activity of Au/MnO_2-R catalyst is also much higher than the activities of Au/TiO_2, Au/Fe_2O_3, and Au/C reference gold catalysts under similar reaction conditions. This demonstrates that the supports play an essential role for gold catalysts in the alcohol oxidation reaction due to synergetic effects between Au and carriers.

The catalytic performance of the Au/MnO_2-R catalyst was also compared with other reported catalysts in the solvent-free aerobic oxidation of 1-phenylethanol. It should be noted that the experimental conditions in the literatures concerning the selective oxidation of alcohols may deviate from each other. Nevertheless, a rough comparison is still feasible in the present study. As shown in Table 3, the Au/MnO_2-R catalyst shows higher TOF than the literature results[21,57,58] in the solvent-free oxidation of 1-phenylethanol, except that for the Au−Pd/TiO_2

TABLE 3: Comparison of the Catalytic Performance of Au/MnO_2-R Catalyst with That of Other Catalysts Employed in the Aerobic Oxidation of 1-Phenylethanol to Acetophenone

catalyst	1-phenylethanol TOF (h^{-1})	selectivity (%)	P_{O2} (atm)	temperature (°C)	solvent	ref
Au/MnO_2-R	15 760[a]	>99	1	160	none	this work
Au/$Cu_5Mg_1Al_2O_x$	11 748	>99	1	160	none	21
Au−Pd/TiO_2	269 000		1	160	none	19
Au/CeO_2	12 500	>99	1	160	none	57
Pd/hydroxyapatite	9 800		1	160	none	58

[a] Reaction conditions: 1 atm of O_2 (60 mL·min^{-1}), 10 mg of catalyst, 200 mmol of substrate. The turnover frequency (TOF) for the oxidation of 1-phenylethanol was calculated by dividing the initial reaction rate during the first hour of the reaction to the number of gold atoms.

catalyst,[19] demonstrating that the present catalytic system can serve as a promising catalyst for the selective oxidation of alcohols.

3.4. Discussion. Manganese dioxide is traditionally used as a versatile stoichiometric oxidation reagent for the direct oxidation of alcohols to aldehydes or ketones.[48] However, the low oxidation efficiency and pollution issues associated with the byproducts from both economical and ecological points of view make it less attractive in the oxidation procedures. In the present study, we have shown experimentally that by incorporation of gold nanoparticles, the stoichiometric oxidation sites on MnO_2 can be converted into catalytic sites for the selective oxidation of alcohols. In particular, by using MnO_2 nanorods as support materials exceptionally high activity in the liquid-phase aerobic oxidation of alcohols has been achieved over the Au/MnO_2-R catalyst. Note that the commercial MnO_2 has a relatively lower BET surface area (5 $m^2 \cdot g^{-1}$) compared with MnO_2 nanorods (10 $m^2 \cdot g^{-1}$); however, this difference does not seem to impose considerable effects on the resulting gold loading, phase structure, and size distribution of gold nanoparticles for the two catalysts, as indicated by the combined elemental analysis and TEM results. It should also be mentioned that it is unlikely the surface contamination of the MnO_2 support due to different preparation history may contribute to some extent to the superior performance of the present Au/MnO_2-R sample, since no sulfur or other remnants could be detected by XPS measurements on the surface of the MnO_2 nanorod materials. Consequently, the key role of the surface structural properties of the support in determining the catalytic performances of the gold catalysts could be established.

The performance of catalysts depends strongly on their surface structures, which have a direct relationship with the crystal planes or crystal phases.[48−50] In this sense, rational design of catalysts with desirable properties, i.e., high activity and selectivity, should involve the fabrication of well-defined reactive crystal planes.[51] In this study, both XRD and TEM results reveal a predominant exposure of the {110} plane in the β-MnO_2 nanorod material, whereas a significant fraction of more closely compact facets are expected for the commercial β-MnO_2 particles.[52] We propose that this great diversity in the surface morphology of the support accounts for the different redox properties and catalytic behaviors of the two gold catalysts. The β-MnO_2 (pyrolusite) has a rutile-type structure with tetragonal symmetry, with the oxygen ions forming a distorted hexagonal close packing array.[53] Previously, on the basis of a thorough theoretical calculation of the electrostatic potential, Woning and van Santen predict that the rutile (110) surface can be reduced easier than the anatase (101) surface.[54] Moreover, a recent theoretical study of the oxygen adsorption on three planes (001), (110), and (111) of β-MnO_2 has shown that the (110) plane has the highest reactivity toward the activation of oxygen molecules.[55] On the basis of these results, we infer that the β-MnO_2 nanorods bear more reactive surfaces as compared with the commercial MnO_2 particles.

More importantly, it should be noted that introducing Au to MnO_2 produces a strong Au−MnO_2 interaction. The different surface structural features clearly determine the strength of metal−support interaction and thus the catalytic activity. TPR results indicate that the introduction of gold results in much lower reduction temperature for Au/MnO_2-R than that of Au/MnO_2-C. Stobbe et al. have suggested that the reducibility of manganese oxide is determined by its crystallinity or defect concentration rather than the oxidation state.[32] This is consistent with the findings derived from the analysis of O 1s XPS spectra (Table 1) which reveal the presence of more oxygen defects on the surface of MnO_2 nanorods supported gold catalyst. It is likely that the introduction of Au to MnO_2 may reduce the barrier for the creation of an oxygen vacancy that is most likely adjacent to the Au sites.[56] Alternatively, the MnO_2 support materials are activated by the incorporation of gold, to a larger extent for Au/MnO_2-R catalyst. The XPS results also reveal that higher fraction of oxidized Au species are present on the MnO_2 nanorod supports before and after the reaction, compared with the gold catalyst supported on commercial MnO_2. According to the reaction mechanism for aerobic oxidation of alcohols proposed by Abad et al.,[57] the activation of oxygen molecules takes place at the oxygen defect sites on the surface of the support, while the positive gold ions play an important role in the rate-determining step involving the hydride shift from the alcohol to gold. Therefore, the presence of more oxygen vacancies and oxidized gold species is considered to be the key point in relation to the excellent activity of the Au/MnO_2-R catalyst for the aerobic oxidation of alcohols, although many details of the mechanism still remain unraveled.

4. Conclusions

In this study, gold nanoparticles were deposited on two MnO_2 materials with different morphologies, i.e., particles and well-defined nanorods, by the HDP method. It is shown that the two types of gold catalysts have similar gold loading and gold particle size distributions. TPR results revealed that the presence of gold significantly promotes the reduction of the MnO_2 nanorods. XPS revealed both reduced and oxidized Au species on the MnO_2 nanorod supports before and after the reaction. The catalysts were tested in the liquid-phase aerobic oxidation of benzyl alcohol under solvent-free conditions. The catalytic activity tests show that the gold supported on MnO_2 nanorods is much more active than that on the commercial MnO_2 particles. The far superior catalytic performance of gold supported on MnO_2 nanorods is attributed to the collaborative effects resulting from beneficial interaction between the electronically modified Au nanoparticles and the well-defined reactive surface of nanorods.

Acknowledgment. This work was supported by the NSF of China (20421303, 20473021, and 20633030), the State Key Basic Research Program of PRC (2003CB615807), the National High Technology Research and Development Program of China (2006AA03Z336), the Shanghai Science and Technology Committee (07QH14003), and the Shanghai Education Committee (06SG03).

References and Notes

(1) Haruta, M. *Catal. Today* **1997**, *36*, 153.
(2) Bond, G. C.; Thomson, D. T. *Catal. Rev. Sci. Eng.* **1999**, *41*, 319.
(3) Hashmi, A. S. K.; Hutchings, G. J. *Angew. Chem., Int. Ed.* **2007**, *45*, 7896.
(4) Min, B. K; Friend, C. M. *Chem. Rev.* **2007**, *107*, 2709.
(5) Grunwaldt, J. D.; Kiener, C.; Wögerbauer, C.; Baiker, A. *J. Catal.* **1999**, *181*, 223.
(6) Grunwaldt, J. D.; Baiker, A. *J. Phys. Chem. B* **1999**, *103*, 1002.
(7) Sanchez-Castillo, M. A.; Couto, C.; Kim, W. B.; Dumesic, J. A. *Angew. Chem., Int. Ed.* **2004**, *43*, 1140.
(8) Schubert, M. M.; Hackenberg, S.; van Veen, A. C.; Muhler, M.; Plzak, V.; Behm, R. J. *J. Catal.* **2001**, *113*, 197.
(9) Baumweda, G. R.; Tsubota, S.; Nakamura, T.; Haruta, M. *Catal. Lett.* **1997**, *44*, 83.
(10) Minico, S.; Scire, S.; Crisafulli, C.; Visco, A. M.; Galvagno, S. *Catal. Lett.* **1997**, *47*, 273.
(11) Molina, L. M.; Hammer, B. *Phys. Rev. Lett.* **2003**, *90*, 206102.
(12) Sanchez, A.; Abbet, S.; Heiz, U.; Schneider, W. D.; Hakkinen, H.; Barnett, R. N.; Landman, U. *J. Phys. Chem. A* **1999**, *103*, 9573.
(13) Lemire, C.; Meyer, R.; Shaikhutdinov, S.; Freund, H. J. *Angew. Chem., Int. Ed.* **2003**, *43*, 118.
(14) Lopez, N.; Nørskov, J. K. *J. Am. Chem. Soc.* **2002**, *124*, 11262.
(15) Mills, G.; Gordon, M. S.; Metiu, H. *Chem. Phys. Lett.* **2002**, *359*, 493.
(16) Porta, F.; Prati, L. *J. Catal.* **2004**, *224*, 397.
(17) Abad, A.; Concepcion, P.; Corma, A.; Garcia, H. *Angew. Chem., Int. Ed.* **2005**, *44*, 4066.
(18) Enache, D. I.; Knight, D. W.; Hutchings, G. J. *Catal. Lett.* **2005**, *103*, 43.
(19) Enache, D. I.; Edwards, J. K.; Landon, P.; Solsona-Espriu, B.; Carley, A. F.; Herzing, A. A.; Watanabe, M.; Kiely, C. J.; Knight, D. W.; Hutchings, G. J. *Science* **2006**, *311*, 362.
(20) Choudhary, V. R.; Dhar, A.; Jana, P.; Jha, R.; Uphade, B. S. *Green Chem.* **2005**, *7*, 768.
(21) Haider, P.; Baiker, A. *J. Catal.* **2007**, *248*, 175.
(22) Singoredjo, L.; Korver, R.; Kapteijn, F.; Moulijn, J. *Appl. Catal., B* **1992**, *1*, 297.
(23) Morales, F.; de Smit, E.; de Groot, F. M. F.; Visser, T.; Weckhuysen, B. M. *J. Catal.* **2007**, *246*, 91.
(24) Xia, G. G.; Yin, Y. G.; Willis, W. S.; Wang, J. Y.; Suib, S. L. *J. Catal.* **1999**, *185*, 91.
(25) Radhakrishnan, R.; Oyama, S. T. *J. Phys. Chem. B* **2001**, *105*, 4245.
(26) Han, Y. F.; Chen, F.; Zhong, Z.; Ramesh, K.; Chen, L.; Widjaja, E. *J. Phys. Chem. B* **2006**, *110*, 24450.
(27) Sanchez, R. M. T.; Ueda, A.; Tanaka, K.; Haruta, M. *J. Catal.* **1997**, *168*, 125.
(28) Wang, X.; Li, Y. D. *Chem. Eur. J.* **2003**, *9*, 300.
(29) Zanella, R.; Giorgio, S.; Henry, C. R.; Louis, C. *J. Phys. Chem. B* **2002**, *106*, 7634.
(30) Bond, G. C.; Louis, C.; Thompson, D. T. *Catalysis by Gold*; Imperial College Press: London, 2006; p 113.
(31) Xu, R.; Wang, X.; Wang, D.; Zhou, K.; Li, Y. *J. Catal.* **2006**, *237*, 426.
(32) Stobbe, E. R.; de Boer, B. A.; Geus, J. W. *Catal. Today* **1999**, *47*, 161.
(33) Trevino, H.; Lei, G. D.; Sachtler, W. M. H. *J. Catal.* **1995**, *154*, 245.
(34) Epling, W. S.; Hoflund, G. B.; Weaver, J. F.; Tsubota, S.; Haruta, M. *J. Phys. Chem.* **1996**, *100*, 9929.
(35) Minicò, S.; Scire, S.; Crisafulli, C.; Galvagno, S. *Appl. Catal., B* **2001**, *34*, 277.
(36) Soares, J. M. C.; Morrall, P.; Crossley, A.; Harris, P.; Bowker, M. *J. Catal.* **2003**, *219*, 17.
(37) Fan, L.; Ichikuni, N.; Shimazu, S.; Uematsu, T. *Appl. Catal., A* **2003**, *246*, 87.
(38) Hutchings, G. J.; Hall, M. S.; Carley, A. F.; Landon, P.; Solsona, B. E.; Kiely, C. J.; Herzing, A.; Makkee, M.; Moulijn, J. A.; Overweg, A.; Fierro-Gonzalez, J. C.; Guzman, J.; Gates, B. C. *J. Catal.* **2006**, *242*, 71.
(39) Kapteijn, F.; van Langeveld, A. D.; Moulijn, J. A.; Andreini, A.; Vuurman, M. A.; Turek, A. M.; Jehng, J. M.; Wachs, I. E. *J. Catal.* **1994**, *150*, 94.
(40) Srinivasan, B.; Gardner, S. D. *Surf. Interface Anal.* **1998**, *26*, 1035.
(41) Gardner, S. D.; Hoflund, G. B.; Davidson, M. R. *Langmuir* **1991**, *7*, 2140.
(42) Lee, S. J.; Gavriilidis, A.; Pankhurst, Q. A.; Kyek, A.; Wagner, F. E.; Wong, P. C. L.; Yeung, K. L *J. Catal.* **2001**, *200*, 298.
(43) Peña, D. A.; Uphade, B. S.; Smirniotis, P. G. *J. Catal.* **2004**, *221*, 421.
(44) Choudhary, V. R.; Jha, R.; Jana, P. *Green Chem.* **2007**, *9*, 267.
(45) Dimitratos, N.; Villa, A.; Wang, D.; Porta, F.; Su, D.; Prati, L. *J. Catal.* **2006**, *244*, 113.
(46) Conventional active manganese oxide has been most commonly used as the stoichiometric metal oxidants for the direct oxidation of alcohols to aldehydes or ketones. The reactivity of active manganese oxide is dependent on preparation methods, compositions, and structure. Complicated preparation methods are often necessary, and the use of freshly made active manganese oxide is required.
(47) Au and Mn leaching were negligible during the recycling experiments. Both the Au and Mn concentration in the filtrate is less than 5 ppb as found by ICP.
(48) Son, Y. C.; Makwana, V. D.; Howell, A. R.; Suib, S. L. *Angew. Chem., Int. Ed.* **2001**, *40*, 4280.
(49) Zhou, K.; Wang, X.; Sun, X.; Peng, Q.; Li, Y. *J. Catal.* **2005**, *229*, 206.
(50) Choudary, B. M.; Mulukutla, R. S.; Klabunde, K. J. *J. Am. Chem. Soc.* **2003**, *125*, 2020.
(51) Schlögl, R.; Abd Hamid, S. B. *Angew. Chem., Int. Ed.* **2004**, *43*, 1628.
(52) Rotzinger, F. P.; Kesselman-Truttmann, J. M.; Hug, S. J.; Shklover, V.; Gra1tzel, M. *J. Phys. Chem. B* **2004**, *108*, 5004.
(53) Thackeray, M. M. *Prog. Solid State Chem.* **1997**, *25*, 1.
(54) Woning, J.; van Santen, R. A. *Chem. Phys. Lett.* **1983**, *101*, 541.
(55) Li, L.; Wei, Z. D.; Li, L. L.; Sun, C. X. *Acta Chim. Sin.* **2006**, *64*, 287.
(56) Widmann, D.; Leppelt, R.; Behm, R. J. *J. Catal.* **2007**, *251*, 437.
(57) Abad, A.; Almela, C.; Corma, A.; García, H. *Tetrahedron* **2006**, *62*, 6666.
(58) Mori, K.; Yamaguchi, K.; Hara, T.; Mizugaki, T.; Ebitani, K.; Kaneda, K. *J. Am. Chem. Soc.* **2002**, *124*, 11572.